ARCHIVOS DE LA SOCIEDAD ESPAÑOLA DE OFTALMOLOGÍA

www.elsevier.es/oftalmologia

Original article

Ganglion cell layer analysis with deep learning in glaucoma diagnosis☆

Valentín Tinguaro Díaz-Alemán[a,*], *Francisco José Fumero Batista*[b], *Silvia Alayón Miranda*[b], *Denisse Ángel Pereira*[a], *Víctor Javier Arteaga-Hernández*[a], *José Francisco Sigut Saavedra*[b]

[a] *Unidad de Glaucoma, Servicio de Oftalmología, Hospital Universitario de Canarias, Santa Cruz de Tenerife, Spain*
[b] *Departamento de Ingeniería Informática y de Sistemas, Facultad de Física, Universidad de La Laguna, Santa Cruz de Tenerife, Spain*

ARTICLE INFO

Article history:
Received 25 May 2020
Accepted 16 September 2020
Available online 4 March 2021

Keywords:
Glaucoma
Deep learning
Tomography
Ganglion cells

ABSTRACT

Objective: To determine and compare the diagnostic precision in glaucoma of two deep learning models using infrared images of the optic nerve, eye fundus, and the ganglion cell layer (GCL).

Methods: We have selected a sample of normal and glaucoma patients. Three infrared images were registered with a spectral-domain optical coherence tomography (SD-OCT). The first corresponds to the confocal scan image of the fundus, the second is a cut-out of the first centered on the optic nerve, and the third was the SD-OCT image of the GCL. Our deep learning models are developed on the MatLab platform with the ResNet50 and VGG19 pre-trained neural networks.

Results: 498 eyes of 298 patients were collected. Of the 498 eyes, 312 are glaucoma and 186 are normal. In the test, the precision of the models was 96% (ResNet50) and 96% (VGG19) for the GCL images, 90% (ResNet50) and 90% (VGG19) for the optic nerve images and 82% (ResNet50) and 84% (VGG19) for the fundus images. The ROC area in the test was 0.96 (ResNet50) and 0.97 (VGG19) for the GCL images, 0.87 (ResNet50) and 0.88 (VGG19) for the optic nerve images, and 0.79 (ResNet50) and 0.81 (VGG19) for the fundus images.

Conclusions: Both deep learning models, applied to the GCL images, achieve high diagnostic precision, sensitivity and specificity in the diagnosis of glaucoma.

☆ Please cite this article as: Díaz-Alemán VT, Fumero Batista FJ, Alayón Miranda S, Pereira DÁ, Arteaga-Hernández VJ, Sigut Saavedra JF. Análisis de la capa de células ganglionares con *deep learning* en el diagnóstico de glaucoma. Arch Soc Esp Oftalmol.2021;96:181–188.

* *Corresponding author.*
E-mail address: vtdac@hotmail.com (V.T. Díaz-Alemán).

Análisis de la capa de células ganglionares con *deep learning* en el diagnóstico de glaucoma

Palabras clave:
Glaucoma
Aprendizaje profundo
Tomografía
Células ganglionares

R E S U M E N

Objetivo: Determinar y comparar la precisión diagnóstica en glaucoma de dos modelos de aprendizaje profundo, usando imágenes en infrarrojo del nervio óptico, del fondo de ojo y de la capa de células ganglionares (CCG).

Métodos: Hemos seleccionado una muestra de pacientes normales y con glaucoma. Se recogieron tres imágenes en infrarrojo con un tomógrafo de coherencia óptica de tipo spectral-domain (SD-OCT). La primera corresponde a la imagen de barrido confocal del fondo de ojo, la segunda es un recorte de la primera centrada en el nervio óptico, y la tercera fue la imagen del corte SD-OCT de la CCG. Nuestros modelos de aprendizaje profundo se desarrollaron en la plataforma MATLAB con las redes neuronales preentrenadas ResNet50 y VGG19.

Resultados: Se recogieron 498 ojos de 298 pacientes. De los 498 ojos, 312 son glaucomatosos y 186 son normales. En la prueba, la precisión de los modelos fue de 96% (ResNet50) y 96% (VGG19) para las imágenes de la CCG, de 90% (ResNet50) y 90% (VGG19) para las imágenes del nervio óptico y de 82% (ResNet50) y 84% (VGG19) para las de fondo de ojo. El área ROC en la prueba fue de 0,96 (ResNet50) y 0,97 (VGG19) para las imágenes de la CCG, de 0,87 (ResNet50) y 0,88 (VGG19) para las imágenes del nervio óptico, y de 0,79 (ResNet50) y 0,81 (VGG19) para las imágenes de fondo de ojo.

Conclusiones: Los dos modelos de aprendizaje profundo analizados, aplicados sobre las imágenes de la CCG, ofrecen una alta precisión diagnóstica, sensibilidad y especificidad en el diagnóstico de glaucoma.

Introduction

Glaucoma is the leading cause of irreversible blindness worldwide. Approximately 80 million people[1] are affected by glaucoma, and it is estimated that 112 million will have the disease by 2040[2]. However, several surveys suggest that most glaucoma patients do not know they have the disease[3,4]. There are several reasons for this phenomenon, including limited knowledge of the disease[4,5] and the fact that the first symptoms of glaucoma do not appear until very advanced stages[6].

Since the last decade, the diagnosis of glaucoma has improved with the introduction of optical coherence tomography (OCT), which has become a necessary tool for quantifying morphological damage to the optic nerve in patients with glaucoma[7]. Both the measurement of the thickness of the peripapillary fiber layer and of the neuroretinal ring fibers by OCT have proved to be reproducible and sensitive in the diagnosis of glaucoma, also enabling to determine the presence of progression and to establish a rate of change[8–10]. Finally, OCT has also shown that damage to the ganglion cell layer (GCC) is prevalent among patients with incipient glaucoma[11,12] and therefore is useful for the diagnosis and control of progressive change in glaucoma patients[13]. The glaucomatous lesion in this layer presents as patterns with different intensities and color shades (RGB) and shape, depending on the density of cells, with the lower temporal thinning being the most frequent[14].

Recently, deep learning models have been applied with great diagnostic precision, sensitivity and specificity in the screening of diabetic retinopathy, based on color retinographies[15,16]. These techniques have also demonstrated their usefulness in the identification of optic nerves with glaucomatous damage using retinography[17,18]. The diagnosis of glaucoma involves several challenges: while in the diagnosis of diabetic retinopathy a series of well-established patterns are analyzed (microaneurysms, hard exudates, etc.), the diagnosis of glaucoma is more complex because patterns suggestive of glaucoma may be present in normal people but their morphology may change in relation to the severity of the disease, and they may even be absent or practically imperceptible to the ophthalmologist in early stages of the disease. Finally, their study must be supplemented with data from clinical examinations, with functional and structural tests. All this constitutes a diagnostic challenge for the clinician and for deep learning models.

The authors propose that GCC images may be more useful because the lesion patterns in this layer are based on changes in color tone and intensity, are usually asymmetrical to hemiretin and have no morphological structures to analyze. This could favor the diagnosis of glaucoma through deep learning. Therefore, the main objective of this work is to compare accuracy in the diagnosis of glaucoma of infrared images of the GCC, the optic nerve and the fundus using these techniques.

Currently, there is not much literature that applies deep learning models of GCC imaging for glaucoma diagnosis, so

we consider this approach quite novel. Only one recent related work, by Lee et al. has been found, in which a model was developed to predict the density of the ganglion cell layer and the internal plexiform. In this work a good correlation was obtained between the prediction of the model and OCT[19].

Methods

In order to carry out this work, a sample of normal and glaucoma patients from the database of patients who attend outpatient clinics at the Glaucoma Unit of the Ophthalmology Service of the University Hospital of the Canary Islands during the year 2019 were retrospectively selected. The protocol of this work was evaluated and approved by the Research Ethics Committee of the authors' hospital and all methods adhere to the principles of the Declaration of Helsinki for research with patients.

The selection of the patients was made by a member of the research team with more than 10 years of experience in the field of glaucoma. Patients with a diagnosis of primary or secondary open-angle glaucoma with untreated intraocular pressure greater than 21 mmHg were included. The diagnosis of glaucoma was based on the presence of reproducible defects in the white-white perimetry and/or morphological criteria based on a spectral domain optical coherence tomograph SD-OCT Spectralis (Heidelberg Engineering, GmbH, Dossenheim, Germany) with the Glaucoma Premium and Posterior Pole module. The morphological criteria of glaucoma were the following: significant changes in neuroretinal ring thickness together with significant changes in the peripapillary nerve fiber layer measured at 3.5 mm and hemirretinal asymmetry in the GCC. Both eyes were included if they met the inclusion criteria.

All patients with concomitant ocular pathology other than glaucoma, lower visual acuity of 20/40, refractive error greater than five diopters of spherical equivalent or three diopters of astigmatism, level of false positives, negatives and fixation errors equal to or greater than 25% in the visual field were excluded from the study. Patients with hypoplastic or oblique optic nerves were also excluded.

Three images were collected with a Spectralis SD-OCT. The first correspond to the confocal scanning image of the fundus in infrared (815 nm), the second is a clipping of the first centered on the optic nerve and the third is the SD-OCT clipping image (880 nm) of the GCC, with density represented by changes in color intensity (RGB) (Fig. 1). The images were extracted raw, with a minimum quality index of 20. Data on age, sex, eye (right/left), intraocular pressure (IOP), and mean defect (MD) were collected from the patients using an Octopus 301 campimeter (Haag-Streit AG, Köniz, Switzerland) with TOP strategy.

For deep learning analysis the MATLAB platform was used (Massachusetts, USA). MATLAB (short for *MATrix LABoratory*, matrix laboratory) is a numerical computing system that provides an integrated development environment with a proprietary programming language (M language). Its basic features include matrix manipulation, data and function representation, algorithm implementation, user interface (GUI) creation, and communication with programs in other languages and with other *hardware* devices. In addition, the capabilities of MATLAB can be extended with toolboxes. One such toolbox is the *deep learning toolbox,* which provides an environment for designing and implementing deep neural networks.

Table 1 – Study demographics.

	Glaucoma	Normal	Meaning
Eyes	312	186	
Age	68.1 (12.7*)	53 (16.9)	$p < 0.001$
MD (dB)	10.6 (7.5)	2.03 (4.4)	$p < 0.001$
IOP (mmHg)	30.8 (5.6)	16.3 (2.9)	$p < 0.001$
Male sex	165	68	$p < 0.001$

* The numbers in parentheses represent the standard deviation.

There are several types of deep neural networks. Convolutional neural networks are of greater interest for the present study due to being the most suitable type for working on images. Their architecture is specially designed to recognize specific elements in the images, and to process them faster.

Two pre-trained convolutional networks were used in the MATLAB environment, i.e. ResNet50 and VGG 19. ResNet50 comprises 50 layers, and VGG19 has 19.

In order to be processed, the images were scaled to a resolution of 224×224 pixels. 80% of the image sample was randomly selected for training and network validation, and the remaining 20% for testing. The data augmentation technique was used to increase the number of images in the sample, by means of random transformations that would provide new images with a consistent appearance with the originals. This reduces the possibility of overfitting and allows the network to learn the most relevant features. Overfitting occurs when the trained model is too close to the input data, and therefore is not able to make good predictions later. A larger set of input data makes this phenomenon more difficult.

During the training process the internal parameters of the model are adjusted iteratively. In our case, the models were trained with a *miniBatchSize of* 10 (number of images used for each update of the model parameters) and a *LearnRate of* 3e-4 (value that limits the magnitude of the modifications that can be made to the internal parameters of the model in each iteration). Under these conditions the two models were trained three times, once for each group of images in the study.

The accuracy, sensitivity and specificity of the system was calculated for each image group and model. We used the area under the curve (ROC) with 95% confidence intervals to evaluate the performance of the models.

Results

The study samplecomprised 498 eyes from 298 patients. Of the 498 eyes, 312 had glaucoma and 186 were normal. The average age of the sample was 62.4 years (SD 16.18). The MD of the eyes with glaucoma was 10.6 dB (SD 7.5) and of the normal eyes was 2.03 dB (SD 4.4). Of the glaucomas, 112 were classified as mild (MD 2.86 dB), 72 as moderate (MD 8.79 dB) and 128 as advanced (MD 18.42 dB). Table 1 shows the demographic data and clinical characteristics of the study sample.

Table 2 – Accuracy, sensitivity, specificity and ROC area of ResNet50 and VGG19.

	GCC		Optic nerve		Fundus	
	ResNet50	VGG19	ResNet50	VGG19	ResNet50	VGG19
Accuracy (training)	92.13%	95.51%	92.14%	93.26%	89.89%	92.13%
Accuracy (test)	96%	96%	90%	90%	82%	84%
Sensitivity	96.80%	93.50%	100%	96.80%	90.30%	93.50%
Specificity	94.70%	100%	73.75%	78.60%	68.40%	68.40%
ROC (test)	0.96	0.97	0.87	0.88	0.79	0.81
ROC 95% CI	0.94–0.98	0.95–0.99	0.86–0.88	0.87–0.89	0.78–0.80	0.80–0.82

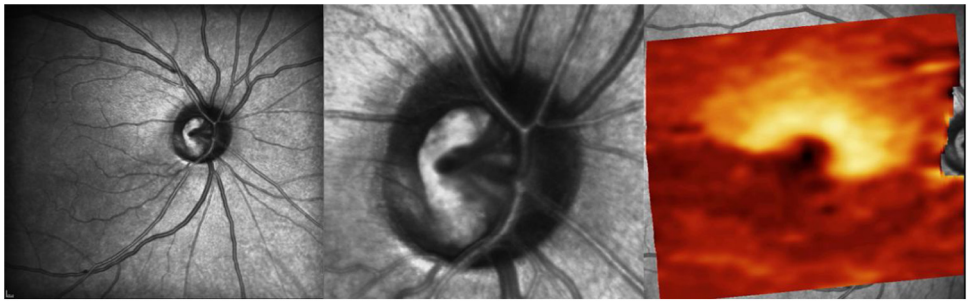

Fig. 1 – Confocal image in background infrared (left), of the optic nerve (center) and the layer of ganglion cells (right), corresponding to a glaucoma patient included in the study.

In training, the models achieved diagnostic accuracy for GCC images of 92.13% (ResNet50) and 95.51% (VGG19), for optic nerve images of 92.14% (ResNet50) and 93.26% (VGG19), and for background images of 89.89% (ResNet50) and 92.13% (VGG19). During the test, the accuracy of the models was 96% (ResNet50) and 96% (VGG19) for GCC images, 90% (ResNet50) and 90% (VGG19) for optic nerve images and 82% (ResNet50) and 84% (VGG19) for fundus images. The sensitivity and specificity values and ROC area of the models are shown in Table 2.

The two models have the best ROC areas and the best ratio between sensitivity and specificity with GCC images: ROC 0.96 (ResNet50), ROC 0.97 (VGG19), sensitivity 96.80% (ResNet50), 93.50% (VGG19), and specificity 94.70% (ResNet50), 100% (VGG19). As can be seen in Table 2, the specificity data of the two models with the fundus image group are lower than the other two groups, sensitivity 90.30% (ResNet50), 93.50% (VGG19) and specificity 68.40% (ResNet50 and VGG19). Finally, both models offer very good sensitivity with the optic nerve image group (100% ResNet50 and 96.80% VGG19), but their specificity does not exceed 80%, with an ROC area of 0.87 (ResNet50) and 0.88 (VGG19).

An example of correct classification by our deep learning models is shown in Fig. 2. The upper images (Fig. 2a–c) correspond to GCC images, where a focal loss of ganglion cells can be clearly seen at a lower temporal level. The lower ones (Fig. 2d–f) are images of the optic nerve where an increase of the optic cup is predominant in different stages, with evident nasal rejection of the vascular package.

Fig. 3 shows the cases where the two models made erroneous diagnosis. The possible reasons for these errors will be discussed in detail in the Discussion section.

Discussion

This study investigated the accuracy of two deep learning models in identifying glaucomatous optic neuropathy in infrared images of the GCC, optic nerve and fundus. The two models showed good performance with GCC images, followed by optic nerve and fundus images. Recently, several published papers have reported the use of deep learning for glaucoma evaluation[18,20–22]. Li et al., with a volume of 48,116 color retinographies, reported that the deep learning system achieved 92.9% accuracy and ROC area of 0.98[18]. Ahn et al., using color retinographies and the Inception V3 model, achieved 84.5% accuracy and 0.93[20] ROC area. Shibata et al., working with color images and using the ResNet model, achieved 96% accuracy, with 0.96[21] ROC area. Christopher et al., using preprocessed retinographies to locate and extract the optic nerve, evaluated three different models: VGG16, Inception V3 and ResNet50, with ResNet50 achieving a higher overall ROC area of 0.91[22].

There are several characteristics among the data sets of the cited works that can explain the difference in results vis-a-vis the present study. First, the dataset used in these works is larger than ours. The work of Li et al. contains a greater number of images (48,116 vs. 498) and obtains a greater ROC area and precision (0.98 vs. 0.88) and (92.9% vs. 90%). Due to the high data requirements of deep-learning models, the addition of thousands of background images would substantially improve model performance. Second, the present study uses infrared images instead of color retinographies. Infrared imaging has some advantages over color imaging such as greater penetration of media opacity which makes it suitable for imaging cataract patients[23]. They also have the potential to provide deeper visualization of the retina, as they comprise longer wavelengths, compared to the green channel commonly used in color retinographies[24]. Finally, it has been shown that there is good agreement among researchers in assessing the superficial vasculature of the retina with color retinographies and infrared images[25]. The use of confocal imaging with deep learning models is less developed than the use with color retinography images. The ease of acquisition and lower cost of retinography makes it an excellent method of screening and object analysis. Nevertheless, some authors have worked with confocal imaging. Christopher et al., using a sample of 948 cases of glaucoma with infrared confocal imaging, obtained an ROC area of 0.81 for the overall sample, and 0.92 if only moderate and severe glaucomas were selected for analysis[26]. Despite the difference in sample size, this data is close to ours.

The present study shows that more precision is obtained with the image centered on the optic nerve instead of on the fundus image. This difference between the analyses of the two groups of images can be explained because it is on the region of the optic nerve where the most significant morphological changes of the disease develop. Focusing only on this region allows a better use of glaucomatous patterns and, therefore, better performance[27]. However, an excessive reduction in the field of vision of the models could hinder their ability to learn alternative characteristics not previously valued or known in other regions[28].

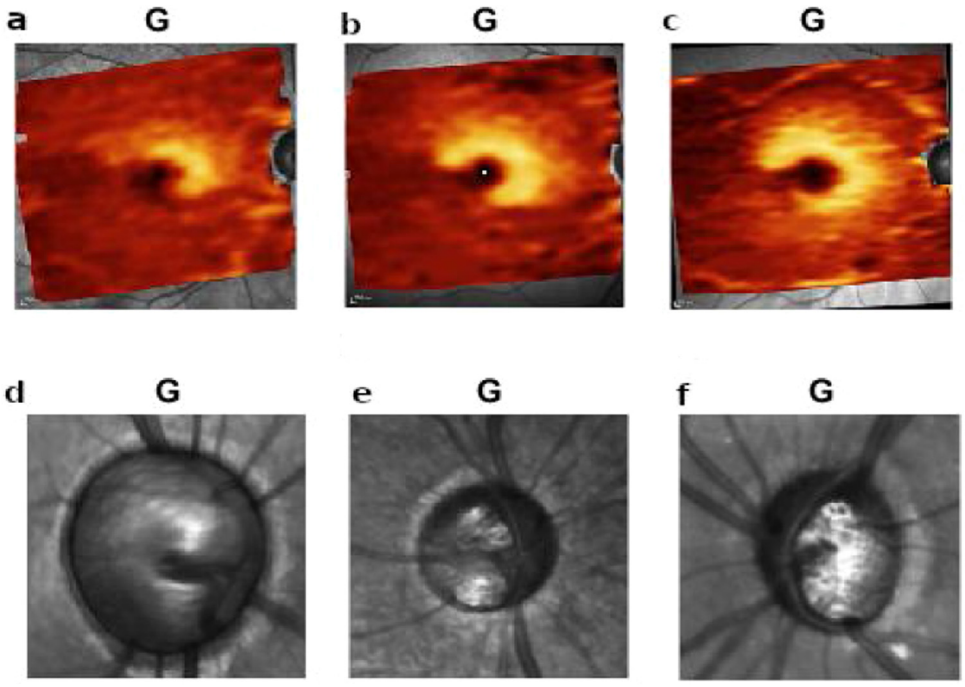

Fig. 2 – GCC and optic nerve images correctly diagnosed by deep learning models. G: glaucoma.

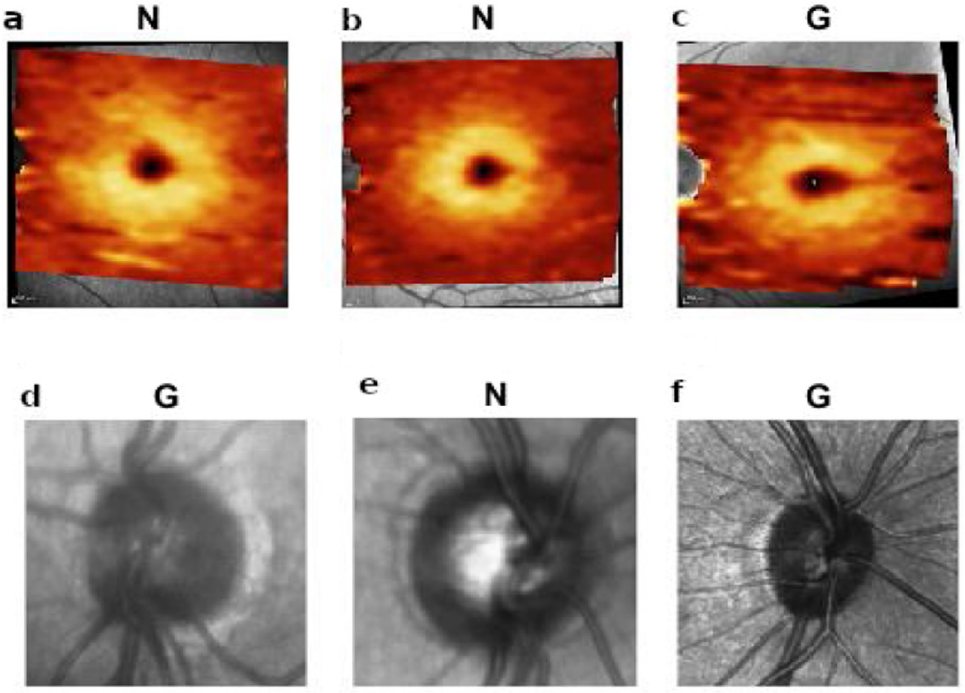

Fig. 3 – Examples of false positives (c, d, f) and negatives (a, b, e) of deep learning models. N: normal; G: glaucoma.

The two tested models offer good performance with all three sets of images studied. The best performance is obtained with the GCC images, followed by the optic nerve and fundus images. Specifically, the GCC model VGG19 offers 96% diagnostic accuracy in the test, with an ROC area of 0.97. While these results are superior to those obtained from analysis of optic nerve or fundus images, we must interpret them with caution. The patterns produced by glaucoma in this layer can be focal or diffuse, the most frequent being lower temporary focal loss. These patterns are, in principle, simpler to interpret than those present in images of the optic nerve, where there are various anatomical structures involved in the detection of the lesions. This difference between the number and complexity of the patterns could explain why our models obtain

better accuracy with GCC images. An et al., in 357 eyes and using an OCT device (3D OCT-2000, Topcon Corp, Tokyo, Japan) trained the VGG19 model and found an ROC area of 0.94 for the images centered on the optic nerve and 0.944 for the GCC[29] images. We have obtained a greater difference between the ROC areas by analyzing these two groups of images with the same model. This discrepancy between the results may be due to the difference in sample size between both studies, to the different adjustment parameters of the VGG19 model or to differences in the image due to the fact that the OCT devices of both studies are different.

In what concerns the GCC images misclassified by the networks studied (Fig. 3), a possible reason could be the absence of a focal pattern (Fig. 3a–c). With respect to misclassified cases of the optic nerve, image quality is an important factor. In two cases presented there is a slight blurring of the image and this may be the cause of the error (Fig. 3d, e). In the last case (Fig. 3f), the absence of an optical cup could be another cause of misinterpretation. The optical cup is present in both normal and glaucomatous patients. The increase of the optical cup is a critical sign of glaucoma that deep learning models tend to consider as pathological. However, its absence has been associated with classification errors[30].

Our work has its limitations. The first is the size of the sample. In deep learning models a large sample size would help to improve the performance of the model, decreasing overfitting, making the model more reproducible. Second, another aspect that affects the model is the balance between the samples. In our case, there is a mismatch between the number of patients with glaucoma and normal subjects. Despite these two limitations, the models were able to learn because the precision values, both in training and in testing, are very close for GCC and optic nerve images.

Conclusion

In conclusion, the results of the present study suggest that deep learning analysis of the infrared images of the optic nerve, the fundus and the GCC are useful in the diagnosis of glaucoma. In the analysis with our two models, the GCC achieved high diagnostic precision, sensitivity and specificity in the diagnosis of glaucoma, followed by the images of the optic nerve and the fundus.

Funding

This study has not received any funding.

Conflict of interests

No conflict of interests was declared by the authors.

REFERENCES

1. Quigley HA, Broman AT. The number of people with glaucoma worldwide in 2010 and 2020. Br J Ophthalmol. 2006;90:262–7, http://dx.doi.org/10.1136/bjo.2005.081224.
2. Tham YC, Li X, Wong TY, Quigley HA, Aung T, Cheng CY. Global prevalence of glaucoma and projections of glaucoma burden through 2040: a systematic review and meta-analysis. Ophthalmology. 2014;121:2081–90, http://dx.doi.org/10.1016/j.ophtha.2014.05.013.
3. Budenz DL, Barton K, Whiteside-de Vos J, Schiffman J, Bandi J, Nolan W, et al. Prevalence of glaucoma in an urban West African population: the Tema Eye Survey. JAMA Ophthalmol. 2013;131:651–8, http://dx.doi.org/10.1001/jamaophthalmol.2013.1686.
4. Hennis A, Wu SY, Nemesure B, Honkanen R, Leske MC, Barbados Eye Studies Group. Awareness of incident open-angle glaucoma in a population study: the Barbados Eye Studies. Ophthalmology. 2007;114:1816–21, http://dx.doi.org/10.1016/j.ophtha.2007.06.013.
5. Sathyamangalam RV, Paul PG, George R, Baskaran M, Hemamalini A, Madan RV, et al. Determinants of glaucoma awareness and knowledge in urban Chennai. Indian J Ophthalmol. 2009;57:355–60, http://dx.doi.org/10.4103/0301-4738.55073.
6. Weinreb RN, Aung T, Medeiros FA. The pathophysiology and treatment of glaucoma: a review. JAMA. 2014;311:1901–11, http://dx.doi.org/10.1001/jama.2014.3192.
7. Tatham AJ, Medeiros FA. Detecting structural progression in glaucoma with optical coherence tomography. Ophthalmology. 2017;124:S57eS65, http://dx.doi.org/10.1016/j.ophtha.2017.07.015.
8. Leung CK, Cheung CY, Weinreb RN, Qiu Q, Liu S, Li H, et al. Retinal nerve fiber layer imaging with spectral-domain optical coherence tomography: a variability and diagnostic performance study. Ophthalmology. 2009;116:1257–63, http://dx.doi.org/10.1016/j.ophtha.2009.04.013.
9. Dong ZM, Wollstein G, Schuman JS. Clinical utility of optical coherence tomography in glaucoma. Invest Ophthalmol Vis Sci. 2016;57, http://dx.doi.org/10.1167/iovs.16-19933. OCT556-OCT67.
10. Kuang TM, Zhang C, Zangwill LM, Weinreb RN, Medeiros FA. Estimating lead time gained by optical coherence tomography in detecting glaucoma before development of visual field defects. Ophthalmology. 2015;122:2002–9, http://dx.doi.org/10.1016/j.ophtha.2015.06.015.
11. Hood DC, Raza AS, De Moraes CG, Liebmann JM, Ritch R. Glaucomatous damage of the macula. Prog Retin Eye Res. 2013;32:1–21, http://dx.doi.org/10.1016/j.preteyeres.2012.08.003.
12. Hwang YH, Jeong YC, Kim HK, Sohn YH. Macular ganglion cell analysis for early detection of glaucoma. Ophthalmology. 2014;121:1508–15, http://dx.doi.org/10.1016/j.ophtha.2014.02.019.
13. Pazos M, Dyrda AA, Biarnés M, Gómez A, Martín C, Mora C, et al. Diagnostic accuracy of spectralis SD OCT automated macular layers segmentation to discriminate normal from early glaucomatous eyes. Ophthalmology. 2017;124:1218–28, http://dx.doi.org/10.1016/j.ophtha.2017.03.044.
14. Shin JW, Sung KR, Park SW. Patterns of progressive ganglion cell-inner plexiform layer thinning in glaucoma detected by OCT. Ophthalmology. 2018;125:1515–25, http://dx.doi.org/10.1016/j.ophtha.2018.03.052.
15. Sayres R, Taly A, Rahimy E, Blumer K, Coz D, Hammel N, et al. Using a deep learning algorithm and integrated gradients explanation to assist grading for diabetic retinopathy. Ophthalmology. 2019;126:552–64, http://dx.doi.org/10.1016/j.ophtha.2018.11.016.
16. Krause J, Gulshan V, Rahimy E, Karth P, Widner K, Corrado GS, et al. Grader variability and the importance of reference standards for evaluating machine learning models for

diabetic retinopathy. Ophthalmology. 2018;125:1264–72, http://dx.doi.org/10.1016/j.ophtha.2018.01.034.
17. Phene S, Dunn RC, Hammel N, Liu Y, Krause J, Kitade N, et al. Deep learning and glaucoma specialists: the relative importance of optic disc features to predict glaucoma referral in fundus photographs. Ophthalmology. 2019;126:1627–39, http://dx.doi.org/10.1016/j.ophtha.2019.07.024.
18. Li Z, He Y, Keel S, Meng W, Chang RT, He M. Efficacy of a deep learning system for detecting glaucomatous optic neuropathy based on color fundus photographs. Ophthalmology. 2018;125:1199–206, http://dx.doi.org/10.1016/j.ophtha.2018.01.023.
19. Lee J, Kim YK, Ha A, Sun S, Kim YW, Kim JS, et al. Macular ganglion cell-inner plexiform layer thickness prediction from red-free fundus photography using hybrid deep learning model. Sci Rep. 2020;10:3280, http://dx.doi.org/10.1038/s41598-020-60277-y.
20. Ahn JM, Kim S, Ahn KS, Cho SH, Lee KB, Kim US. A deep learning model for the detection of both advanced and early glaucoma using fundus photography. PLoS One. 2018;13:e0207982, http://dx.doi.org/10.1371/journal.pone.0207982.
21. Shibata N, Tanito M, Mitsuhashi K, Fujino Y, Matsuura M, Murata H, et al. Development of a deep residual learning algorithm to screen for glaucoma from fundus photography. Sci Rep. 2018;8:14665, http://dx.doi.org/10.1038/s41598-018-33013-w.
22. Christopher M, Belghith A, Bowd C, Proudfoot JA, Goldbaum MH, Weinreb RN, et al. Performance of deep learning architectures and transfer learning for detecting glaucomatous optic neuropathy in fundus photographs. Sci Rep. 2018;8:16685, http://dx.doi.org/10.1038/s41598-018-35044-9.
23. Kirkpatrick JN, Manivannan A, Gupta AK, Hipwell J, Forrester JV, Sharp PF. Fundus imaging in patients with cataract: role for a variable wavelength scanning laser ophthalmoscope. Br J Ophthalmol. 1995;79:892–9, http://dx.doi.org/10.1136/bjo.79.10.892.
24. Elsner AE, Burns SA, Weiter JJ, Delori FC. Infrared imaging of sub-retinal structures in the human ocular fundus. Vis Res. 1996;36:191–205, http://dx.doi.org/10.1016/0042-6989(95)00100-e.
25. Ajaz A, Aliahmad B, Kumar H, Sarossy M, Kumar DK. Agreement study between color and IR retinal images based on retinal vasculature morphological parameters. BMC Ophthalmol. 2019;19:27, http://dx.doi.org/10.1186/s12886-018-0997-6.
26. Christopher M, Bowd C, Belghith A, Goldbaum MH, Weinreb RN, Fazio MA, et al. Deep learning approaches predict glaucomatous visual field damage from OCT optic nerve head en face images and retinal nerve fiber layer thickness maps. Ophthalmology. 2020;127:346–56, http://dx.doi.org/10.1016/j.ophtha.2019.09.036.
27. Orlando JI, Fu H, Barbosa Breda J, Van Keer K, Bathula DR, Diaz-Pinto A, et al. REFUGE challenge: a unified framework for evaluating automated methods for glaucoma assessment from fundus photographs. Med Image Anal. 2020;59:101570, http://dx.doi.org/10.1016/j.media.2019.101570.
28. Chen X, Xu Y, Wong DWK, Wong TY, Liu J. Glaucoma detection based on deep convolutional neural network. Annu Int Conf IEEE Eng Med Biol Soc. 2015:715–8, http://dx.doi.org/10.1109/EMBC.2015.7318462.
29. An G, Omodaka K, Hashimoto K, Tsuda S, Shiga Y, Takada N, et al. Glaucoma diagnosis with machine learning based on optical coherence tomography and color fundus images. J Healthc Eng. 2019;18:4061313, http://dx.doi.org/10.1155/2019/4061313.
30. Diaz-Pinto A, Morales S, Naranjo V, Köhler T, Mossi JM, Navea A. CNNs for automatic glaucoma assessment using fundus images: an extensive validation. Biomed Eng Online. 2019;18:29, http://dx.doi.org/10.1186/s12938-019-0649-y.